

https://dspace.org/

Dendritefree zinc metal anode for longlife zincion batteries enabled by an artificial hydrophobiczincophilic coating

H Zhang; T Shui; Nosipho Moloto; An Li; Ruogu Zhang ...

https://hdl.handle.net/10539/45857
WOS

Downloaded from a DSpace repository. https://dspace.org/

Journal of Colloid and Interface Science 678 (2025) 1148–1157

Contents lists available at ScienceDirect

Journal of Colloid And Interface Science

journal homepage: www.elsevier.com/locate/jcis

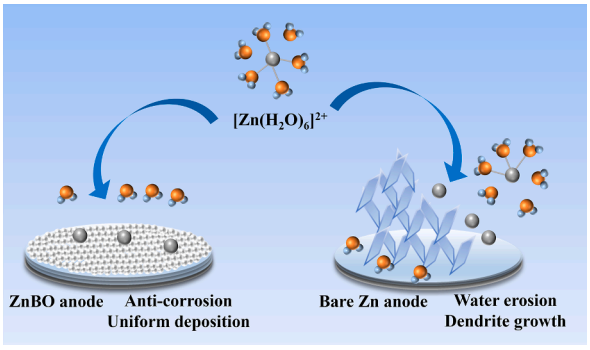
Regular Article

Dendrite-free zinc metal anode for long-life zinc-ion batteries enabled by an artificial hydrophobic-zincophilic coating

Hanning Zhang [a], Tao Shui [a,*], Nosipho Moloto [b], An Li [c], Ruogu Zhang [d], Jiacheng Liu [e], Song-Zhu Kure-Chu [e], Takehiko Hihara [e], Wei Zhang [a,*], ZhengMing Sun [a,*]

[a] School of Materials Science and Engineering, Southeast University, Nanjing 211189, China
[b] Molecular Science Institute, School of Chemistry, University of the Witwatersrand, Private Bag 3, Wits, 2050, South Africa
[c] Analysis and Testing Center, Southeast University, Nanjing 211189, China
[d] Nanjing Jinling High School International Department, No. 169, Zhongshan Road, Gulou District, Nanjing City 210009, China
[e] Department of Materials Function and Design, Nagoya Institute of Technology, Gokiso-cho, Showa-ku, Nagoya, Aichi, 4668555, Japan

GRAPHICAL ABSTRACT



ARTICLE INFO

Keywords:
Hydrophobicity
Zincophilicity
Zinc borate
Dendrite-free anode
Aqueous zinc-ion batteries

ABSTRACT

Considering the desired energy density, safety and cost-effectiveness, rechargeable zinc-ion batteries (ZIBs) are regarded as one of the most promising energy storage units in next-generation energy systems. Nonetheless, the service life of the current ZIBs is significantly limited by rampant dendrite growth and severe parasitic reactions occurring on the anode side. To overcome these issues caused by poor interfacial ionic conduction and water erosion, we have developed a facile strategy to fabricate a uniform zinc borate layer at the zinc anode/electrolyte interface (ZnBO). Such protective layer integrates superhydrophobic-zincopholic properties, which can effectively eliminate the direct contact of water molecules on the anode, and homogenize the interfacial ionic transfer, thereby enhancing the cyclic stability of the zinc plating/stripping. As a result, the as-prepared ZnBO-coated anode exhibits extended lifespan of 1200 h at 1 mA cm^{-2} and demonstrates remarkable durability of 570 h at 20 mA cm^{-2} in Zn||Zn symmetric cells. Additionally, when coupled to an $NH_4V_4O_{10}$ (NVO) cathode, it also delivers a superior cyclability (203.5 mAh/g after 2000 cycles at 5 A/g, 89.3 % capacity retention) in coin full cells and a feasible capacity of 2.5 mAh at 1 A/g after 200 cycles in pouch full cells. This work offers a unique

* Corresponding authors.
E-mail addresses: tshui@seu.edu.cn (T. Shui), w69zhang@seu.edu.cn (W. Zhang), zmsun@seu.edu.cn (Z. Sun).

https://doi.org/10.1016/j.jcis.2024.09.092
Received 26 July 2024; Received in revised form 9 September 2024; Accepted 9 September 2024
Available online 11 September 2024
0021-9797/© 2024 Elsevier Inc. All rights are reserved, including those for text and data mining, AI training, and similar technologies.

perspective on integrating hydrophobicity and zincophilicity at the anode/electrolyte interface through an artificial layer, thereby enhancing the cycle lifespan of ZIBs.

1. Introduction

Rechargeable secondary batteries have emerged as paramount energy storage units, playing a pivotal role in transitioning human society to a new production and living system predominantly powered by electricity [1–4]. Amidst considerations such as safety, resource availability, and cost-effectiveness, aqueous zinc batteries (ZIBs) have earned substantial attention [5–7]. Boasting a substantial capacity of 5855 mAh cm^{-3}, a favorable potential of −0.76 V vs standard hydrogen electrode (SHE), and abundant resource reservoirs, ZIBs have emerged as compelling contenders poised to supplant lithium-ion batteries (LIBs) [8], mitigating the risks of combustion hazards associated with organic electrolytes [9,10]. However, the primary challenges faced by ZIBs predominantly revolve around the zinc metal anode, limiting the lifespan of the batteries [11,12]. These challenges encompass corrosion, hydrogen evolution reactions (HER), and the surface passivation under aqueous conditions over extended cycles, which primarily induce the irreversible consumption and damage of the anode [13,14]. Furthermore, uneven Zn deposition facilitates the proliferation of dendrites, ultimately leading to the separator puncture and ZIB failure [15,16]. Hence, there is an imperative need to develop an effective strategy to achieve advanced cycling durability for the zinc metal anode. The core of the strategy involves optimizing the zinc ion transport process at the anode-electrolyte interface [17], specifically by enhancing the reversibility of the Zn stripping/plating process and avoiding the water molecule erosion of the interface.

To date, a plethora of studies have been conducted to address the anode challenges of ZIBs, ranging from electrolyte composition optimization to electrolyte additive development. These efforts focus on introducing molecules or networks that strongly interact with zinc ions, thereby advancing the solvation structure of plating/striping zinc ions and the interfacial zinc diffusion flux [18–20]. However, as Zn^{2+}-interacting molecules or networks are gradually consumed, the cycling stability of ZIBs decreases, eventually leading to irreversible damage to the anode interface [21]. Additionally, the randomness and complexity of molecular interactions introduce greater uncertainty in the performance and cost of ZIBs [22]. In contrast, constructing artificial interfacial layers offers more controllable, stable, and long-lasting protection for zinc anodes by offering a more direct means of controlling the interfacial deposition environment [23,24]. The ideal artificial interface for an anode could separate zinc ions from aqueous electrolyte molecules and provide an ionic conduction network to facilitate Zn^{2+} transport, optimizing transport while shielding water molecules to improve ZIB performance. [25–27].

In comparison to organic protective layers, inorganic compounds such as TiO_2 [28], $CaCO_3$ [29], and ZrP [30], renowned for their exceptional thermodynamic stability and environmental compatibility, emerge as promising candidates for artificial interface designs. Nevertheless, these compounds often exhibit an elevated repulsive interaction with zinc ions, which can hinder interfacial ion transport and consequently compromise overall performance. In light of this, zincophilicity becomes crucial, as it underpins effective transportation sites and enhances the reversibility of zinc deposition [31]. To meet the required criteria, integrating zinc-containing compounds offer promising approaches. Materials such as ZnTe [32], ZnSe [33], and ZnS [34] have garnered considerable attention for their ability to effectively reduce nucleation potential and provide favorable interaction sites for zinc ions. Artificial interfaces constructed with these compounds have been shown to promote uniform nucleation and promotes the reversibility of Zn plating/stripping, thereby enhancing the overall stability of the ZIBs. However, such interlayers can still facilitate the conduction of water molecules. This conduction may finally induce side reactions at the anode/electrolyte, limiting the cycling lifespan of ZIBs. Therefore, developing an artificial interface layer that integrates both hydrophobic properties and Zn^{2+} affinity holds potentials for addressing the critical challenges faced by zinc anodes in aqueous electrolytes [35,36], promising significant advancements in interfacial engineering for improved battery technologies.

Herein, a superhydrophobic and zincophilic zinc borate (ZnBO) artificial interface was fabricated on the zinc anode using a straightforward spray coating method, as shown in Fig. 1. Due to the Zn^{2+} affinity and water-repellent nature of the ZnBO layer, validated by Contact angle measurements, solvated zinc ions in the electrolyte are directed through the layer to the anode, while water molecules are prevented from penetrating the layer. This regulation of zinc ion flux and effective water shielding lead to dendrite-free anodes and eliminate side reactions. Additionally, the boron-rich phase of the layer promotes uniform electrodeposition and reduces the nucleation barriers for metallic Zn. Such design culminates in exceptional deposition stability (1200 h with ~36 mV voltage hysteresis at 1 mA cm^{-2}) and extends the durability of the Zn anodes at high current density (570 h @ 20 mA cm^{-2} with a cumulative plating capacity of 5.7 Ah cm^{-2}) in the Zn||Zn symmetric cells. Besides, when assembled with the $NH_4V_4O_{10}$ (NVO) cathode, the ZnBO||NVO full cell demonstrates improved capacity retention, maintaining 90% of its capacity after 2000 cycles, compared to a bare Zn full cell. The unique features of this artificial interface design not only exemplify the innovative integration of superhydrophobic and zincophilic properties but also shows the potential to advance the development of ZIBs to new levels.

2. Experimental section

2.1. Materials

$Zn_3B_2O_6$ (99%), ammonium metavanadate (NH_4VO_3), zinc sulfate ($ZnSO_4{\cdot}7H_2O$) and N—N' methylpyrrolidone (NMP) were purchased from Shanghai Aladdin Co. Ltd. Zinc foil (50 μm, 99.99%), Ti foil (10 μm) and Cu foil (11 μm) were purchased from Chengshuo Metal Materials Co., Ltd. The additives, including Super P carbon black and polyvinylidene fluoride (PVDF) were purchased from Nanjing Mojiesi Energy Technology Co., Ltd.

2.2. Preparation of ZnBO anode and bare Zn znode

To obtain the bare Zn anode, the zinc foil was polished with 2000 grit sandpaper to remove a thin layer of surface oxide, followed by ultrasonication with anhydrous ethanol for 5 min to remove impurities.

To obtain the ZnBO anode. Firstly, 180 mg of zinc borate and 20 mg of PVDF were dispersed in 15 mL NMP and stirred for 6 h to form a homogeneous paste. Subsequently, the bare zinc anode was cut into 8*8 cm size and pasted on a heating table and heated up to 230 °C The prepared slurry was uniformly sprayed onto the zinc foil. Finally, the residual solvent was removed by drying in a vacuum oven at 80 °C for 12 h.

2.3. Materials characterization

The chemical composition of the as-prepared anodes was characterized by X-ray diffraction (XRD, Haoyuan DX-2700b, China) and X-ray photonic spectroscopy (XPS, Thermofisher 4800, U.S.A) The morphology of the anode before and after cycle was observed by scanning electron microscope (SEM, FEI Nova, U.S.A) and laser microscope

(LSM, KEYENCE VK-X150, Japan). The contact angle measurement was analyzed via OCA25HTV contact angle measuring instrument (China).

2.4. Electrochemical test

For the zinc plating/stripping stability evaluation, CR-2032 coin-type cells was employed. And the Zn||Zn and ZnBO||ZnBO symmetric cells was assembled, which utilized Whatman GF/D as the separator and the 2 M $ZnSO_4$ as the electrolyte. For the deposition behavior analyzation, including Linear scanning voltametric (LSV), Tafel plots and chronoamperometry (CP) tests, were tested in the three-electrode system using an electrochemical workstation(Biological SP150, France).

For the Zn||Cu half cells evaluations, the Cu foil was used as working electrode, while zinc foil was used as counter and reference electrode. The sepeator and electrolyte was same as the Zn||Zn symmetric cells.

For the full coin cells evaluations, ammonium vanadate ($NH_4V_4O_{10}$, NVO) was performed as the cathode, which was synthesized via conventional hydrothermal method according to the previous work [37], while the NVO cathode was coated on the Ti foils with a mass loading of ~2 mg cm^{-2}. The sepeator and electrolyte was same as the above-mentioned. For the full pouch cells evaluations, the area of both electrodes is 2 × 2.5 cm^2 and the charge/discharge profiles were monitored by the Neware CT-5000 batteries battery test systems (Shenzhen, China), which was tested from 0.2 V to 1.6 V. The cyclic voltammetry (CV) was tested by the biological SP150 electrochemical workstation with a scanning rate of 0.5 mV/s from 0.2 V to 1.6 V. And electrochemical impedance spectroscopy (EIS) was monitored on the same electrochemical workstation from 0.01 to 10^5 Hz with an amplitude of 10 mV, which were tested under the open circuit potential (~1.2 V vs Zn/Zn^{2+}). The ionic conductivity of the different interfaces were conducted by placing the samples into a stainless-steel mold and performing an EIS test, with a calculation based on the following Eq. (1):

$$\sigma = \frac{l}{RA} \tag{1}$$

Where l, A, and R are the thickness, area, and resistance of the hydrogel electrolyte, respectively.

2.5. In-situ optical microscopy observation

The in-situ electrochemical deposition process was observed by the Zeiss optical microscope combined with an electrochemical workstation (Biological VSP, France). A homemade battery with transparent quartz window was assembled. All the observations were tested at 10 mA cm^{-2} with an areal capacity of 10 mAh cm^{-2}.

2.6. Computational details

First-principles calculations were conducted using VASP-5.4.4, [38,39] with the Generalized Gradient Approximation (GGA) based on the Perdew-Burke-Ernzerhof (PBE) exchange–correlation functional and the Projector Augmented-Wave (PAW) method.[40,41] A heterostructure was constructed by combining a 2 × 3 supercell of the Zn (1 0 1) surface with the ZBO (1 0 1) surface. The k-point sampling for both the surface and the supercell was performed using the Monkhorst-Pack scheme with a 3 × 4 × 1 grid.[42] A vacuum layer of 15 Å was included to avoid interactions between periodic images. To accurately account for van der Waals interactions, the DFT-D3 correction was applied.[43] The interface energy (E_{int}) of the heterostructure was calculated to quantify the stability of the interface. The interface energy is defined as: $E_{int}=(E_{het}-E_{Zn}-E_{ZBO})/S$, where E_{het} is the total energy of the heterostructure, E_{Zn} and E_{ZBO} are the total energies of the isolated Zn (1 0 1) and ZnBO (1 0 1) surfaces, respectively, and S is the area of the interface. This calculation provides insight into the thermodynamic stability and bonding strength at the interface. The simplified 2D model served for the calculation of the interfacial electric field distribution in terms of COMSOL Multiphysics according to the previous reports [44].

3. Results & discussion

The fabrication of the protective coating is illustrated in Fig. 1, showing the uniform distribution of zinc borate on the zinc anode via a facile spray coating method (Figs. S1 and S2). The morphology of the ZnBO coating is illustrated in Fig. S3, showing that the homogeneous zinc borate particles with an average size of 1.95 ± 0.6 μm are uniformly distributed on the zinc anode. This coating effectively isolates the zinc anode from water molecules, thereby inhibiting side reactions. The morphology of the bare Zn anode and the corresponding elemental mapping after immersion in a conventional electrolyte for 7 days are shown in Fig. S4, demonstrating the accumulation of by-products on the surface, which can impair the reversibility of zinc deposition. In contrast, the zinc borate-coated anode shows minimal damage and fewer by-products, indicating its corrosion resistance properties (Figs. 2a and 2b). Additionally, these results are corroborated by XRD analysis. As depicted in Fig. 2c, the bare Zn anode exhibits a strong peak at 8°, corresponding to the (0 0 1) plane of zinc hydroxide sulfate (ZHS) [45], which could increase interfacial polarization and cause sluggish charge transfer kinetics. In comparison, the ZnBO anode shows almost

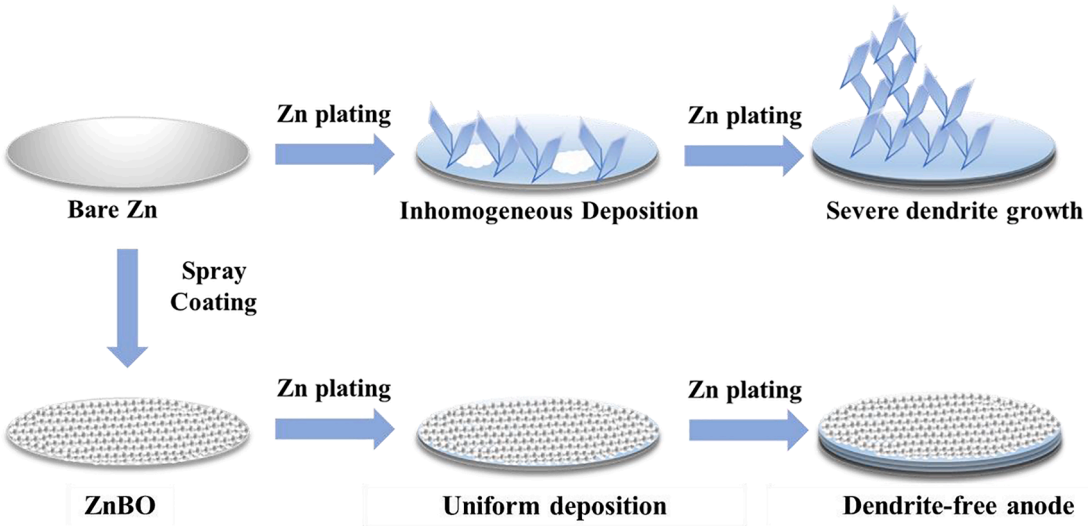


Fig. 1. Schematic illustration of the Zn deposition behavior of ZnBO anode and bare Zn anode.

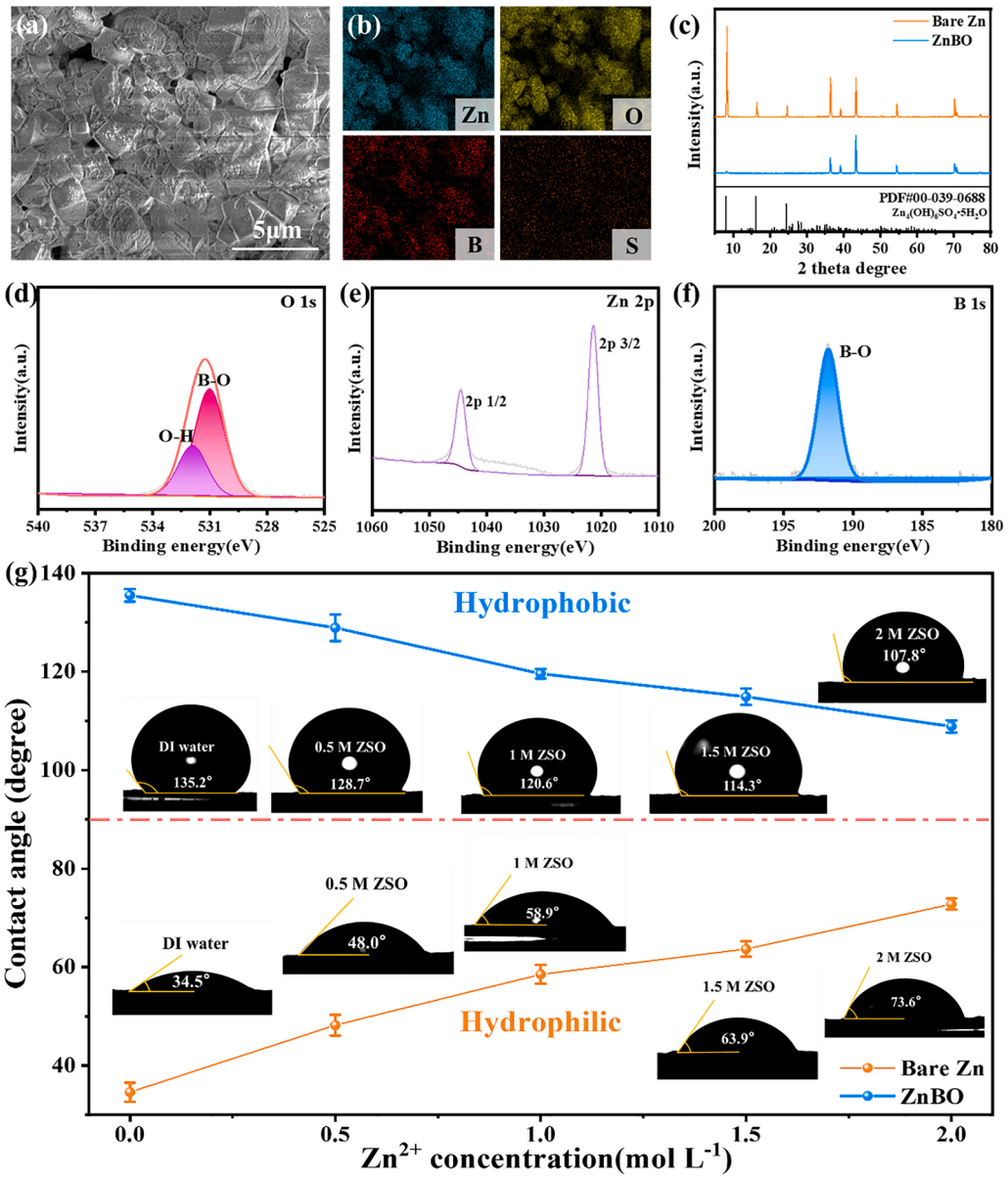


Fig. 2. SEM image of ZnBO anode after immersed in 2 M $ZnSO_4$ electrolyte for 7 days. (b) EDS mapping of the ZnBO anode immersed in 2 M $ZnSO_4$ electrolyte for 7 days. (c) XRD patterns of the bare Zn and ZnBO anodes in 2 M $ZnSO_4$ electrolyte for 7 days. High-resolution XPS spectra of (d) O 1s, (e) Zn 2p, (f) B 1s of the ZnBO anode. (g) Contact angle measurements of ZnBO anode and bare Zn anode with DI water, 0.5 M, 1 M, 1.5 M and 2 M $ZnSO_4$ electrolyte, respectively.

no characteristic peaks of ZHS, proving its inhibition of side reactions (Fig. 2c). Furthermore, the chemical composition of the coating was analyzed using XPS. The peaks at 530.9 and 532.8 eVs correspond to the B-O and O—H bonds in the O 1s spectra (Fig. 2d) [46,47]. The peaks of metallic Zn are observed at 1045.1 and 1023.4 eVs in the Zn 2p spectra (Fig. 2e) [48], with no zinc oxide production observed. In the B 1s spectra, the B-O bond is identified at 192.6 eVs (Fig. 2f) [49]. These results confirm the formation of a B-rich coating that facilitates ionic transfer and promotes nucleation. Furthermore, a comparison of the ionic conductivity with and without the coating confirmed that the introduction of the coating does not impair ion transport at the anode/electrolyte interface (Fig. S5).

To reveal the interaction of the interface with water molecules and zinc ions, contact angle measurements were performed. According to the theoretical model of the dynamic spreading of a droplet on a flat substrate, the diffusion process of the droplets is driven by intermolecular forces between the water molecules and the substrate material. Stronger attractive interactions between the aqueous solution and the substrate surface facilitates a more efficient spreading of droplets, which is reflected in the apparent contact angles [50–52]. To ensure the reproducibility of the test, three experiments were conducted for each group. As illustrated in Fig. 2g, when in contact with DI water, the ZnBO anode exhibits a notable hydrophobicity with a high contact angle of 135.2 ± 0.3°. However, as the zinc ion concentration increases, the contact angle gradually decreases to 107.8 ± 0.2° but remains above 90°, confirming that the ZnBO coating retains its hydrophobicity while exhibiting a strong affinity for zinc ions. The superior ionic conductivity of ZnBO (40.56 mS cm^{-1}) further demonstrates that this fabricated hydrophobic layer helps in enhancing the transport of hydrated zinc ions. This indicates that zincophilicity and hydrophobicity can synergistically protect the zinc anode. In contrast, the bare Zn anode exhibits hydrophilic properties with a contact angle of 48.0 ± 0.4° for DI water. With the addition of ZSO, the contact angle shows a marked increase (Fig. 2h). This increase is attributed to the electrostatic adsorption of hydrophilic hydroxyl groups and anionic species (e.g., SO_4^{2-}) on the zinc anode surface, which occupy hydrogen bonding sites and reduce hydrophilicity

[53–55]. Moreover, the adsorbed anionic groups attract zinc ions, leading to the accumulation of zinc sulfate (ZSO) on the zinc surface, which could promote the anode side reactions, such as dendrite growth and surface passivation, during electrochemical cycling. Compared with the reported anode protection strategy [56] which focused on fabricating hydrophilic coatings to accelerate Zn^{2+} transport and adjust solvation structure, we have developed a hydrophobic and zincophilic zinc borate layer on the zinc anode. The zincophilic nature of the coating layer enhances the interfacial transport of zinc ions and optimizes Zn^{2+} flux distributions. Simultaneously, the hydrophobic property of the coating promotes zinc ion desolvation and inhibit interfacial side reactions caused by water molecules, which were overlooked in previous studies. Also, contact angle measurements showed that the contact angle of ZnBO layer continuously decreases with increasing zinc ion concentration but remains above 90°, confirming that the ZnBO coating retains its hydrophobicity while exhibiting a strong affinity for zinc ions. This indicates that zincophilicity and hydrophobicity can synergistically protect the zinc anode. The demonstration of this synergistic effect and the corresponding coating fabrication have not been previously reported, underscoring the novelty of this work".

To reveal the component of SEI, the XPS spectra of the ZnBO anode after cycling are shown in Fig. S6. The C-F bond peak at 687.2 eV in the F 1s spectra indicates that the PVDF remains intact after cycling [3] (Fig. S6a), whereas the peak at 530.3 eV in the O 1s spectrum corresponds to the formation of Zn-O bonds [17] (Fig. S6b). Additionally, the B-O bond is observed in the B 1s spectrum at 192.2 eV [46,47] (Fig. S6c), suggesting the formation of Zn-O-B ligands. This formation facilitates the desolvation of zinc ions and inhibits the creation of by-products. Furthermore, the nanoindentation curve of the ZnBO anode, shown in Fig. S7 (Supporting Information), reveals a hardness of 37 MPa and an elastic modulus of 1.79 GPa. This indicates that the ZnBO anode exhibits excellent durability in inhibiting zinc dendrite growth.

To evaluate the zinc deposition behavior of different samples, Chronoamperometry (CA) curves are presented in Fig. 3a. The ZnBO anode maintains a stable current density of 14.6 mA cm^2, while the bare Zn anode shows a continuous increase, reaching 57.7 mA cm^2. This indicates that the zinc borate coating introduces an additional energy barrier, which inhibits the aggregation of zinc crystal nuclei and promotes more uniform deposition. The nucleation overpotential (NOP) of different samples is shown in Fig. 3b, demonstrating that the zinc borate coating reduces the NOP from 53 mV to 15 mV. Furthermore, the linear polarization (LP) curves reveal that the ZnBO anode exhibits superior corrosion resistance, with a lower corrosion current density of 0.94 mA cm^2 compared to the bare Zn anode (2.48 mA cm^{-2}, Fig. 3c). The linear scanning voltammetry (LSV) curves are presented in Fig. 3d. The ZnBO anode has a negative shift in the HER onset potential (−1.70 V vs. Ag/AgCl) compared to bare ZnSO4 (−1.65 V vs. Ag/AgCl), indicating that the zinc borate coating effectively inhibits the hydrogen evolution reaction (HER).

To visualize the promotion of uniform zinc deposition facilitated by the coating, in-situ optical microscopy (OM) was employed. As illustrated in Fig. 3e, the ZnBO anode exhibits uniform deposition with no observable dendrite growth. The corresponding SEM image and the 3D reconstruction from the laser scanning microscopy (LSM) image of the ZnBO anode after deposition further reveal a dense and homogeneous morphology (Figs. 3f and 3g). In contrast, the bare Zn anode exhibits significant inhomogeneous deposition (Fig. 3h), and the SEM image reveals highlighting pronounced dendrite growth (Fig. 3i). Additionally, the 3D reconstruction LSM image displays a notable uneven height difference (Fig. 3j). These observations indicate that the zinc borate coating effectively regulates zinc-ion flux and provides protection against water erosion.

DFT calculations were employed to investigate the mechanism by which the ZnBO layer promotes stable deposition at the interface. As shown in Fig. 4a, the interface structure, interfacial energy (γ), and Young's modulus (E) of the ZnBO anode indicate that the coating possesses superior mechanical properties, effectively suppressing dendrite growth. Additionally, the H adsorption free energy (ΔG) of the ZnBO and bare Zn anodes are presented in Fig. 4b. The ZnBO anode exhibits a higher ΔG of 1.662 eV compared to 0.425 eV for the bare Zn anode, suggesting that the ZnBO anode has a stronger ability to inhibit H_2 evolution. The electrical field distribution at the anode/electrolyte interfaces was further validated via finite element simulation (FEM), as illustrated in Figs. 4c and 4d. Compared to the bare zinc sample, the ZnBO anode displays a more uniform electric field distribution, indicating that the coating mitigates the risk of dendrite growth associated

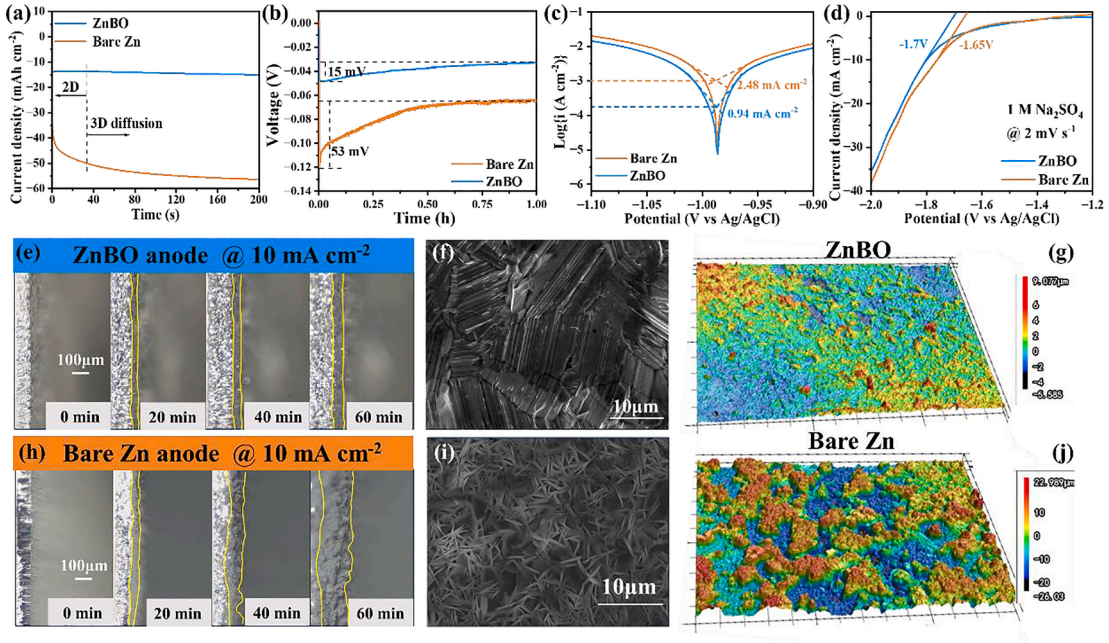


Fig. 3. (a) chronoamperometry curves, (b) NOP curves, (c) Tafel plots and (d) Liner scanning voltametric curves of the bare Zn anode and ZnBO anode. (e) In-situ Cross-sectional optical microscopy image of ZnBO anode plating and (f) corresponding SEM image and (g) 3D reconstruction of LSM image. (h) In-situ Cross-sectional optical microscopy image of bare Zn anode plating and (i) corresponding SEM image and (j) 3D reconstruction of LSM image.

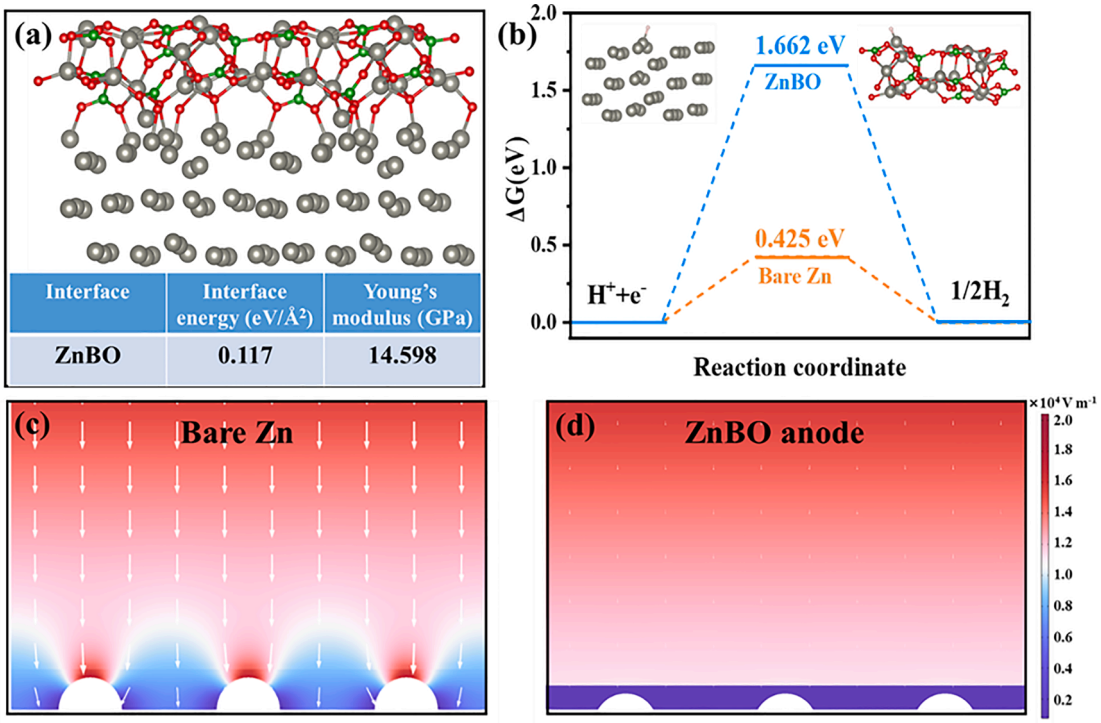


Fig. 4. (a) Interface structure, interfacial energy (γ), and Young's modulus (E) of ZnBO anode. (b) Free-energy diagram on the ZnBO and bare Zn surfaces for HER Finite element simulation results of electric field distribution of (c) bare Zn and (d) ZnBO at anode/electrolyte interface.

with localized electric field inhomogeneities.

Benefiting from the synergistic effects of hydrophobicity and zincophilicity, the ZnBO anode exhibited enhanced reversibility in Zn||Zn symmetric cells. The cross-sections of ZnBO anodes with various coating thicknesses are shown in Fig. S8 (Supporting Information). To determine the impact of coating thickness, ZnBO||ZnBO symmetric cells with varying coating thicknesses were assembled to evaluate their cyclability. As shown in Fig. S9 (Supporting Information), the ZnBO anode with a 10 μm coating exhibited the longest cyclic lifespan, establishing 10 μm as the optimal thickness. Additionally, it was observed that voltage hysteresis increased significantly with increasing coating thickness beyond 10 μm, resulting in rapid deterioration of the cyclic lifespan. This suggests that excessively thick coatings may raise the diffusion energy barrier for zinc ions, leading to inhomogeneous zinc deposition. However, a coating thickness of less than 10 μm is insufficient to effectively shield water molecules and regulate zinc ion transport, resulting in decreased stability at the zinc anode interface and reduced cycling performance. As shown in Fig. 5a, the ZnBO||ZnBO cell demonstrated reduced voltage hysteresis (103 mV at 20 mA cm^{-2}). The incorporation of the zinc borate coating also significantly improved stability, extending the cyclic lifespan to 1200 h at 1 mA cm^{-2} approximately 12 times longer than that of the bare Zn anode (Fig. 5b). Moreover, the ZnBO anode displayed remarkable durability at a high current density of 20 mA cm^{-2}, achieving a cyclic life of 570 h with a cumulative plating capacity (CPC) of 5.7 Ah cm^{-2} (Fig. 5c). Corresponding post-mortem SEM images of the different samples are illustrated in the inset images. The bare Zn anode exhibited severe dendrite growth, leading to battery failure. In contrast, the ZnBO anode displayed a relatively smooth surface, indicating that the ZnBO coating can mitigate side reactions and regulate ion flux, thereby promoting uniform zinc deposition. Compared to other coatings such as ZnPO or PMMA, our approach integrates both hydrophobicity and zincophilicity, demonstrating competitive CPC (Fig. 5d and Table S1). The coulombic efficiency (CE) of the zinc plating/stripping process was assessed using Zn||Cu half-cells, as illustrated in Fig. 5e. Due to the regulation of zinc-ion flux and suppression of side reactions by the zinc borate coating, the Zn||Zinc borate@Cu sample exhibits a higher initial coulombic efficiency (ICE) of 94.46% and an enhanced cyclability of 750 cycles at 5 mA cm^{-2}, with an average CE (ACE) of 99.29%. In contrast, the Zn||Cu sample demonstrated a lower ICE of 89.16% and a reduced cyclic life of 400 cycles, indicating that, without the zinc borate coating, side reactions significantly impair the reversibility of zinc plating. The corresponding charge/discharge profiles, shown in Figs. 5f and S10, further illustrate that the zinc borate coating promotes efficient ion transfer and uniform zinc deposition, resulting in a lower polarization voltage of 103 mV compared to the Zn||Cu half-cell (151 mV).

To assess the practical applications of the zinc borate coating, the prepared anode was paired with conventional ammonium vanadate ($NH_4V_4O_{10}$, NVO), synthesized via the hydrothermal method as described in the previous work (Fig. S11) [37]. The CV curves of the bare Zn||NVO and ZnBO||NVO full cells are presented in Fig. 6a, demonstrating that the zinc borate coating enhances the platform capacity. The Nyquist plots in Fig. 6b reveal that the zinc borate coating reduces the R_{ct} from 104.6 Ω to 52.1 Ω, indicating improved interfacial charge transfer efficiency. Due to the development of the superhydrophobic-zincophilic coating, the ZnBO||NVO full cell demonstrates superior rate performance, delivering specific capacities of 478.3, 445.0, 406.8, 357.3, 271.3, and 182.2 mAh/g at current densities of 0.2, 0.5, 1, 2, 5, and 10 A/g, respectively. In contrast, the bare Zn||NVO full cell shows significantly lower capacities of 60.1 and 33.1 mAh/g at 5 and 10 A/g (Figs. 6c and 6d), respectively. Furthermore, the cyclic performance of the full cells is shown in Fig. 5e. The ZnBO||NVO full cell maintains a specific capacity of 203.5 mAh/g after 2000 cycles at 5 A/g, with a capacity retention of 89.3%. Conversely, the bare Zn||NVO full cell suffers from continuous degradation, retaining only 17.3% of its initial capacity, highlighting the zinc borate coating's effectiveness in mitigating the consumption of active Zn and enhancing cyclability (Fig. 6e). Additionally, the cyclic performance of the ZnBO||NVO pouch cells is shown in Fig. 6f, which delivers a capacity of 2.5 mAh at 1 A/g after 200 cycles with a capacity retention of 83.3%, demonstrating great practical feasibility. In contrast, the Zn||NVO full pouch cells only yields a capacity of 1.6 mAh after 200 cycles, with a low-capacity retention of 64%.

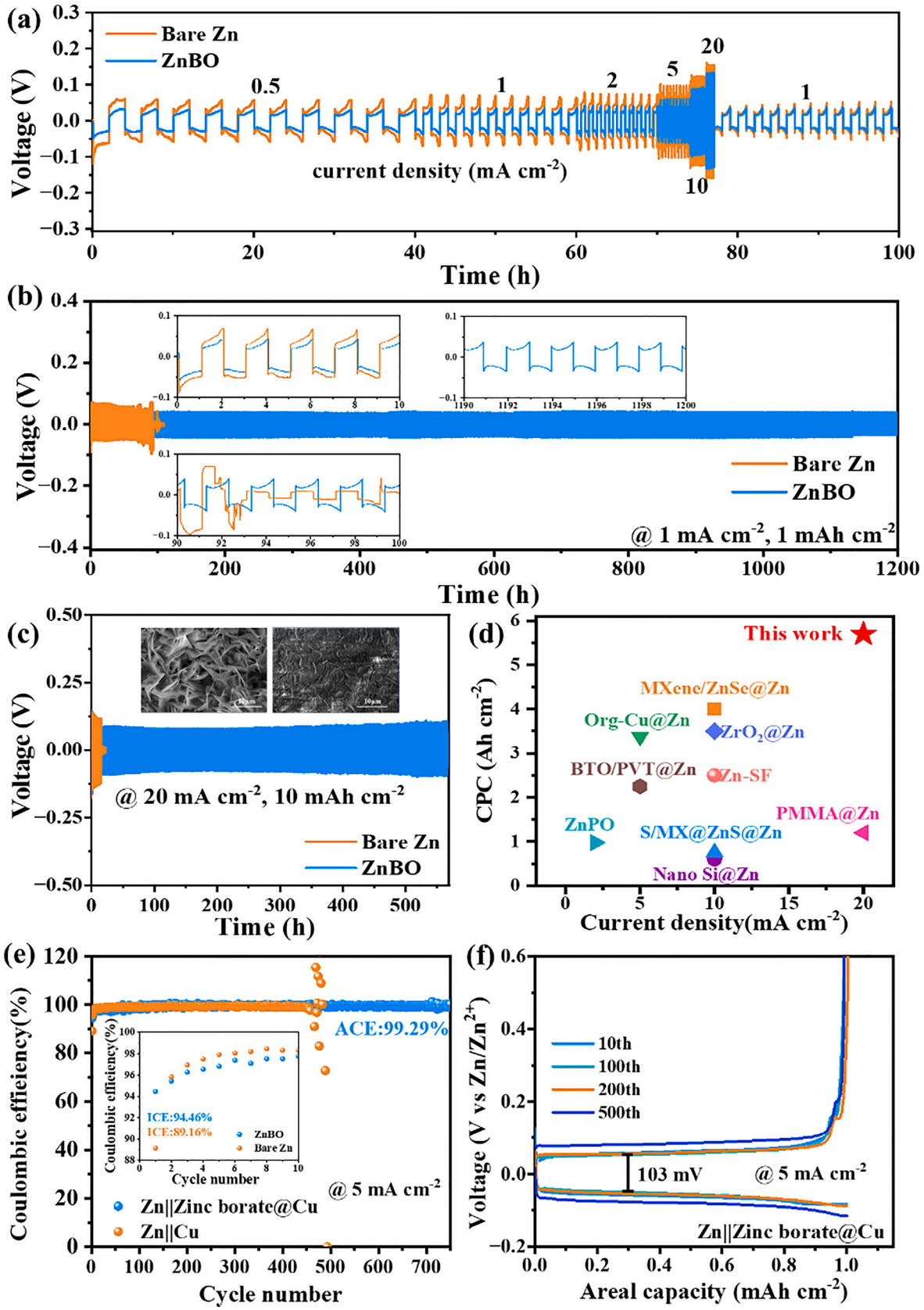


Fig. 5. (a) Rate Capability of the Zn||Zn and ZnBO||ZnBO symmetric cells. Long term cycliability of different samples (b) at 1 mA cm^{-2} with an areal capacity of 1 mAh cm^{-2} and (c) 20 mA cm^{-2} with an areal capacity of 10 mAh cm^{-2}, the inset SEM images illustrated the post-mortem SEM images of the different samples. (d) Comparison of the cumulative plating capacity (CPC) of the previous reports about surface coating design. (e) Long-term plating/stripping cyclic performance of the Zn||Cu half cells at 5 mA cm^{-2}. (f) Charge/discharge profiles of the Zn||ZnBO@Cu half cells at different cycles.

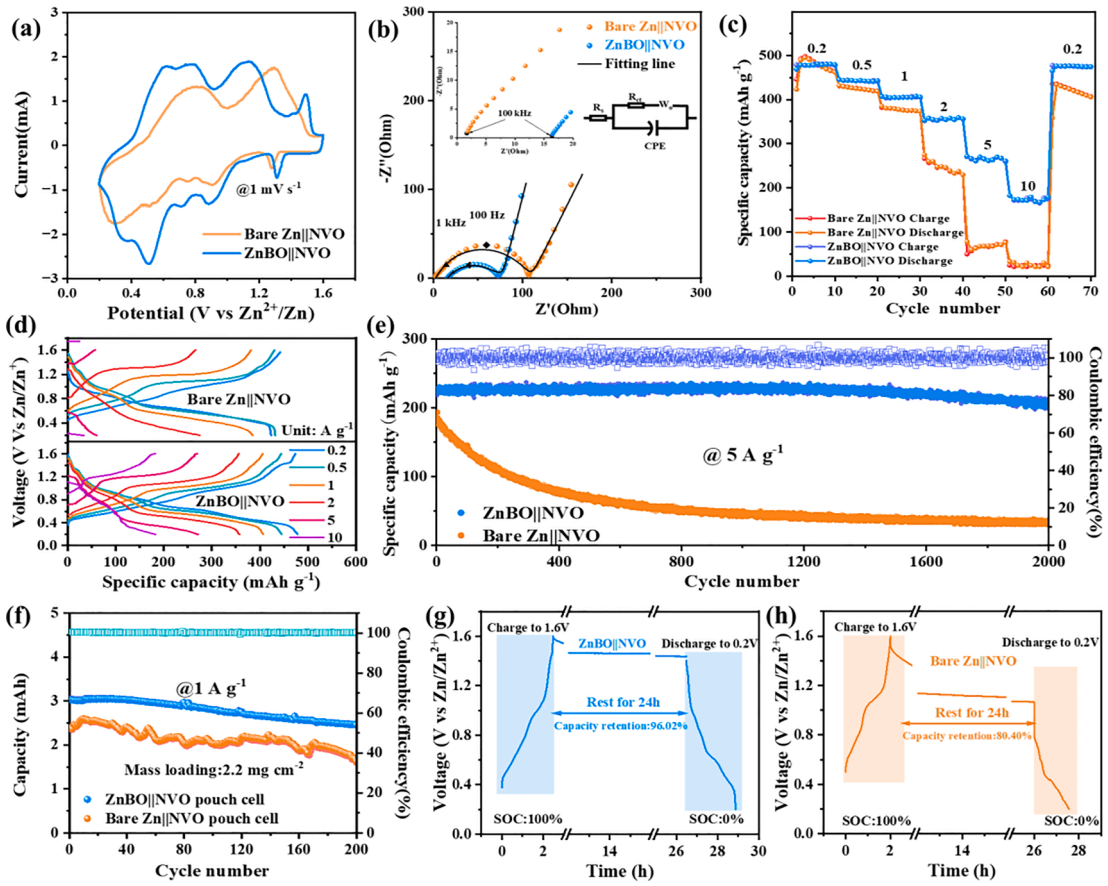


Fig. 6. (a) CV curves of the bare Zn||NVO and ZnBO||NVO full cells at 1 mV/s. (b) Nyquist plots of different samples and corresponding fitting lines and equivalent circuit diagram. (c) Rate capability and (d) corresponding charge/discharge profiles of the bare Zn||NVO and ZnBO||NVO full cells from 0.2 to 10 A/g. (e) Long-term cyclic performance of two samples at 5 A/g. (f) Cyclability of ZnBO||NVO and Zn||NVO full pouch cells at 1 A/g. Storage performances of Zn||NVO full cells based on (g) ZnBO anode and (h) bare Zn anode.

Even at a high mass loading of 11.75 mg cm^{-2}, the ZnBO||NVO full pouch cell delivers a capacity of 6.4 mAh after 150 cycles at 1 A/g, demonstrating significant potential for practical applications (Fig. S12). The ability of the coating to suppress full cell self-discharge was evaluated, as depicted in Figs. 6g and 6h. Compared to the bare Zn||NVO sample, which exhibits a limited capacity retention of 80.4%, the zinc borate coating effectively mitigates the impact of interfacial side reactions, resulting in a superior capacity retention of 96.02%.

4. Conclusion

To adjust the solvation structure of zinc ions and regulate the ion flux at the anode-electrolyte interface, zincophilic artificial interlayers are commonly investigated for anode protection in ZIBs. However, these approaches often overlook the potential side reactions and active zinc consumption caused by water molecules diffusing into the interlayer. To achieve long-lasting ZIBs, a facile spray coating method was developed to produce a zinc borate interlayer on the zinc anode, which exhibits both water repellency and a notable affinity for zinc ions. This dual functionality advances the interfacial zinc ion transport while completely blocking water molecules from eroding the anode. As a result, the ZnBO anode maintained stable performance for 1200 h at 1 mA cm^{-2} and demonstrated remarkable durability for 570 h at 20 mA cm^{-2} in symmetric cells, with a high cumulative plating capacity (CPC) of 5.7 Ah cm^{-2}. Furthermore, when paired with the NVO cathode, the ZnBO||NVO full cell achieved an excellent cyclic lifespan, demonstrating 2000 cycles at 5 A/g with 89.3% capacity retention in coin cells, and a capacity of 2.5 mAh at 1 A/g after 200 cycles in pouch cells. This work introduces a novel approach by leveraging hydrophobicity and zincophilicity to simultaneously alter the kinetic behavior of water molecules and zinc ions via the artificial interlayer, enhancing the reversibility of the zinc anode and offering new perspectives for the development of high-performance zinc-ion batteries.

CRediT authorship contribution statement

Hanning Zhang: Writing – original draft, Methodology, Investigation, Data curation, Conceptualization. **Tao Shui:** Writing – review & editing, Writing – original draft, Validation, Supervision, Formal analysis. **Nosipho Moloto:** Methodology, Investigation. **An Li:** Methodology, Investigation, Data curation. **Ruogu Zhang:** Methodology, Investigation, Formal analysis, Data curation. **Jiacheng Liu:** Methodology, Investigation. **Song-Zhu Kure-Chu:** Methodology, Data curation. **Takehiko Hihara:** Methodology, Investigation. **Wei Zhang:** Writing – review & editing, Validation, Supervision, Methodology, Investigation. **ZhengMing Sun:** Writing – review & editing, Validation, Supervision, Methodology.

Declaration of competing interest

The authors declare that they have no known competing financial interests or personal relationships that could have appeared to influence the work reported in this paper.

Data availability

The authors do not have permission to share data.

Acknowledgments

This work was supported by the National Key Research and Development Program of China (No. 2023YFC3009502), the National Natural Science Foundation of China (No.52371134, No.U23A20574, No.22408047), the Natural Science Foundation of Jiangsu Province (No. BK20231432), Aeronautical Science Foundation of China (2023Z015069001), the Fundamental Research Funds for the Central Universities (No. 2242023K40027), the Start-up Research Fund of Southeast University (RF1028623040) and the SEU Innovation Capability Enhancement Plan for Doctoral Students (CXJH_SEU 24151).

Appendix A. Supplementary data

Supplementary data to this article can be found online at https://doi.org/10.1016/j.jcis.2024.09.092.

References

[1] W. Du, E.H. Ang, Y. Yang, Y. Zhang, M. Ye, C.C. Li, Challenges in the material and structural design of zinc anode towards high-performance aqueous zinc-ion batteries, Energy Environ. Sci 13 (2020) 3330–3360.
[2] H. Jia, Z. Wang, B. Tawiah, Y. Wang, C.-Y. Chan, B. Fei, F. Pan, Recent advances in zinc anodes for high-performance aqueous Zn-ion batteries, Nano Energy 70 (2020) 104523.
[3] H. Zhang, W. Zhang, D. Luo, S. Zhang, L. Kong, H. Xia, Q. Xie, G. Xu, Z. Chen, Z. Sun, Stabilizing Solid Electrolyte Interphase on Liquid Metal Via Dynamic Hydrogel-Derived Carbon Framework Encapsulation, Adv. Mater. 36 (2024) 2401234.
[4] F. Tao, Y. Liu, X. Ren, J. Wang, Y. Zhou, Y. Miao, F. Ren, S. Wei, J. Ma, Different surface modification methods and coating materials of zinc metal anode, J. Energy Chem. 66 (2022) 397–412.
[5] Y. Liang, H. Dong, D. Aurbach, Y. Yao, Current status and future directions of multivalent metal-ion batteries, Nat. Energy 5 (2020) 646–656.
[6] J. Shin, J. Lee, Y. Park, J.W. Choi, Aqueous zinc ion batteries: focus on zinc metal anodes, Chem. Sci. 11 (2020) 2028–2044.
[7] Z. Yi, G. Chen, F. Hou, L. Wang, J. Liang, Strategies for the Stabilization of Zn Metal Anodes for Zn-Ion Batteries, Adv. Energy Mater. 11 (2021) 2003065.
[8] L. Ma, M.A. Schroeder, O. Borodin, T.P. Pollard, M.S. Ding, C. Wang, K. Xu, Realizing high zinc reversibility in rechargeable batteries, Nat. Energy 5 (2020) 743–749.
[9] P.T. Xiao, X.R. Yun, Y.F. Chen, X.W. Guo, P. Gao, G.M. Zhou, C.M. Zheng, Insights into the solvation chemistry in liquid electrolytes for lithium-based rechargeable batteries, Chem. Soc. Rev. 52 (2023) 5255–5316.
[10] K. Xu, Li-ion battery electrolytes, Nat. Energy 6 (2021) 763.
[11] C. Xie, S. Liu, Z. Yang, H. Ji, S. Zhou, H. Wu, C. Hu, Y. Tang, X. Ji, Q. Zhang, H. Wang, Discovering the Intrinsic Causes of Dendrite Formation in Zinc Metal Anodes: Lattice Defects and Residual Stress, Angew. Chem. Int. Ed. 62 (2023) 2218612.
[12] C. Xie, Z. Yang, Q. Zhang, H. Ji, Y. Li, T. Wu, W. Li, P. Wu, H. Wang, Designing Zinc Deposition Substrate with Fully Preferred Orientation to Elude the Interfacial Inhomogeneous Dendrite Growth, Research 2022 (2022) 9841343.
[13] Y.C. Chang, G. Prentice, A MODEL FOR THE ANODIC-DISSOLUTION OF THE ZINC ELECTRODE IN THE PREPASSIVE REGION, J. Electrochem. Soc. 136 (1989) 3398–3403.
[14] Z. Cai, J.D. Wang, Y.M. Sun, Anode corrosion in aqueous Zn metal batteries, eScience 3 (2023) 100093.
[15] W. Lu, C. Xie, H. Zhang, X. Li, Inhibition of Zinc Dendrite Growth in Zinc-Based Batteries, Chemsuschem 11 (2018) 3996–4006.
[16] Y. Zuo, K. Wang, P. Pei, M. Wei, X. Liu, Y. Xiao, P. Zhang, Zinc dendrite growth and inhibition strategies, Mater. Today Energy 20 (2021) 100692.
[17] H. Zhang, T. Shui, W. Zhang, Z. Sun, Parallel zinc deposition enabled by diethylene triaminepentaacetic acid induced interfacial complex for dendrite-free zinc metal anode, Energy Storage Mate. 71 (2024) 103595.
[18] C. Guo, J. Zhou, Y. Chen, H. Zhuang, Q. Li, J. Li, X. Tian, Y. Zhang, X. Yao, Y. Chen, S.-L. Li, Y.-Q. Lan, Synergistic Manipulation of Hydrogen Evolution and Zinc Ion Flux in Metal-Covalent Organic Frameworks for Dendrite-free Zn-based Aqueous Batteries, Angew. Chem. Int. Ed. 61 (2022) 2210871.
[19] Q. Hu, J. Hu, F. Ma, Y. Liu, L. Xu, L. Li, S. Zhang, X. Liu, J. Zhao, H. Pang, Redistributing zinc-ion flux by work function chemistry toward stabilized and durable Zn metal batteries, Energy Environ. Sci. 17 (2024) 2554–2565.
[20] K. Kerns, M. Zigo, E.Z. Drobnis, M. Sutovsky, P. Sutovsky, Zinc ion flux during mammalian sperm capacitation, Nat. Commun. 9 (2018) 2061.
[21] Z. He, R. Li, T. Wang, N. Zhao, L. Dai, J. Zhu, L. Wang, Achieving stable zinc metal anodes by regulating ion transfer and desolvation behavior, J. Colloid Interface Sci. 655 (2024) 717–725.
[22] Z. Yan, M. He, A. Hu, M. Liu, J. Chen, J. Liu, N. Chen, L. Cao, B. Li, J. Long, Manipulating hydrogen and coordination bond chemistry for reversible zinc metal anodes, J. Colloid Interface Sci. 650 (2023) 257–265.
[23] S. Ilic, M.J. Counihan, S.N. Lavan, Y. Yang, Y. Jiang, D. Dhakal, J. Mars, E. N. Antonio, L.K. Iglesias, T.T. Fister, Y. Zhang, E.J. Maginn, M.F. Toney, R.F. Klie, J.G. Connell, S. Tepavcevic, Effect of Antisolvent Additives in Aqueous Zinc Sulfate Electrolytes for Zinc Metal Anodes: The Case of Acetonitrile, ACS Energy Lett. 9 (2023) 201–208.
[24] Y. Deng, C. Liu, W. Shen, J. Zou, Z. Xiao, Q. Zhang, Z. Jiang, Y. Li, Fullerenol as a nano-molecular sieve additive enables stable zinc metal anodes, J. Colloid Interface Sci. 674 (2024) 345–352.
[25] S.H. Huh, Y.J. Choi, S.H. Kim, J.S. Bae, S.H. Lee, S.H. Yu, Enabling uniform zinc deposition by zwitterion additives in aqueous zinc metal anodes, J. Mater. Chem. A 11 (2023) 19384–19395.
[26] L.S. Han, Y.M. Guo, F.H. Ning, X.Y. Liu, J. Yi, Q. Luo, B.H. Qu, J.L. Yue, Y.F. Lu, Q. Li, Lotus Effect Inspired Hydrophobic Strategy for Stable Zn Metal Anodes, Advanced Materials 36 (2024) 2308086.
[27] A.B. Zhou, H.R. Wang, F.L. Zhang, X. Hu, Z.H. Song, Y. Chen, Y.X. Huang, Y.H. Cui, Y.X. Cui, L. Li, F. Wu, R.J. Chen, Amphipathic Phenylalanine-Induced Nucleophilic-Hydrophobic Interface Toward Highly Reversible Zn Anode, Nano-Micro Letters 16 (2024) 164.
[28] K.N. Zhao, C.X. Wang, Y.H. Yu, M.Y. Yan, Q.L. Wei, P. He, Y.F. Dong, Z.Y. Zhang, X. D. Wang, L.Q. Mai, Ultrathin Surface Coating Enables Stabilized Zinc Metal Anode, Adv. Mater. Interfaces 5 (2018) 1800848.
[29] L.T. Kang, M.W. Cui, F.Y. Jiang, Y.F. Gao, H.J. Luo, J.J. Liu, W. Liang, C.Y. Zhi, Nanoporous $CaCO_3$ Coatings Enabled Uniform Zn Stripping/Plating for Long-Life Zinc Rechargeable Aqueous Batteries, Adv. Energy Mater. 8 (2018) 1801090.
[30] J.P. Yan, M.H. Ye, Y.F. Zhang, Y.C. Tang, C.C. Li, Layered zirconium phosphate-based artificial solid electrolyte interface with zinc ion channels towards dendrite-free Zn metal anodes, Chem. Eng. J. 432 (2022) 134227.
[31] T.Q. Huang, K. Xu, N. Jia, L. Yang, H.T. Liu, J.X. Zhu, Q.Y. Yan, Intrinsic Interfacial Dynamic Engineering of Zincophilic Microbrushes via Regulating Zn Deposition for Highly Reversible Aqueous Zinc Ion Battery, Adv. Mater. 35 (2023) 2205206.
[32] D.W. Sha, C.J. Lu, R.X. Hu, Z.H. Bao, L. Pan, Z.M. Sun, Exploiting bifunctional ZnTe for Zn anode protection and conversion-type cathode toward compatible aqueous Zn-ion batteries, Energy Storage Mater. 66 (2024) 103228.
[33] Y. Tian, Y.L. An, Y.J. Yang, B.A. Xu, Robust nitrogen/selenium engineered MXene/ZnSe hierarchical multifunctional interfaces for dendrite-free zinc-metal batteries, Energy Storage Mater. 49 (2022) 122–134.
[34] Y.L. An, Y. Tian, C.K. Liu, S.L. Xiong, J.K. Feng, Y.T. Qian, Rational Design of Sulfur-Doped Three-Dimensional $Ti_3C_2T_x$ MXene/ZnS Heterostructure as Multifunctional Protective Layer for Dendrite-Free Zinc-Ion Batteries, ACS Nano 15 (2021) 15259–15273.
[35] Y.H. Lee, Y. Jeoun, S.H. Lee, J.H. Kim, S.Y. Kim, S.H. Yu, K.S. Ahn, Y.E. Sung, Byproduct reverse engineering to construct unusually enhanced protection layers for dendrite-free Zn anode, Chem. Eng. J 464 (2023) 142580.
[36] H. Xia, W. Zhang, C. Miao, H. Chen, C. Yi, Y. Shang, T. Shui, X. Cao, J. Liu, S.-Z. Kure-Chu, F. Liang, N. Moloto, Y. Xiong, T. Hihara, W. Lu, Z. Sun, Ultra-thin amphiphilic hydrogel electrolyte for flexible zinc-ion paper batteries, Energy Environ, Sci, 2024.
[37] C.F. Liu, Y. Zhang, H.H. Cheng, X.X. Cai, D.Z. Jia, H. Lin, "Dual- Engineering" Strategy to Regulate $NH_4V_4O_{10}$ as Cathodes for High-Performance Aqueous Zinc Ion Batteries, Small 19 (2023) 2301870.
[38] H. Kresse, Ab initio molecular-dynamics simulation of the liquid-metal-amorphous-semiconductor transition in germanium, Physical review, B, Condensed Matter 49 (20) (1994) 14251–14269.
[39] F. Kresse, Efficient iterative schemes for ab initio total-energy calculations using a plane-wave basis set, Physical review, B, Condensed Matter 54 (16) (1996) 11169–11186.
[40] G. Kresse, D. Joubert, From ultrasoft pseudopotentials to the projector augmented-wave method, Physical Review B 59 (3) (1999) 1758–1775.
[41] W. Perdew, Accurate and simple analytic representation of the electron-gas correlation energy, Physical review, B, Condensed Matter 45 (23) (1992) 13244–13249.
[42] H.J. Monkhorst, J.D. Pack, Special points for Brillouin-zone integrations, Physical Review B 13 (12) (1976) 5188.
[43] S. Grimme, J. Antony, S. Ehrlich, H. Krieg, A consistent and accurate ab initio parametrization of density functional dispersion correction (DFT-D) for the 94 elements H-Pu, J. Chem. Phys. 132 (15) (2010) 19.
[44] Z.J. Liu, X.F. Zhang, Z.M. Liu, Y. Jiang, D.L. Wu, Y. Huang, Z. Hu, Rescuing zinc anode-electrolyte interface: mechanisms, theoretical simulations and in situ characterizations, Chemical Science 15 (2024) 7010–7033.
[45] Z. Liang, C. Li, D. Zuo, L. Zeng, T. Ling, J. Han, J. Wan, Achieving stable Zn metal anode through novel interface design with multifunctional electrolyte additive, Energy Storage Mater. 63 (2023) 102980.
[46] H. Nohira, W. Tsai, W. Besling, E. Young, J. Petry, T. Conard, W. Vandervorst, S. De Gendt, M. Heyns, J. Maes, M. Tuominen, Characterization of ALCVD-Al_2O_3 and ZrO_2 layer using X-ray photoelectron spectroscopy, J. Non Cryst. Solids 303 (2002) 83–87.
[47] H. Zhang, P. Chen, H. Xia, G. Xu, Y. Wang, T. Zhang, W. Sun, M. Turgunov, W. Zhang, Z. Sun, An integrated self-healing anode assembled via dynamic encapsulation of liquid metal with a 3D $Ti_3C_2T_x$ network for enhanced lithium storage, Energy Environ. Sci. 15 (2022) 5240–5250.

[48] C.L. Wei, H.F. Fei, Y. Tian, Y.L. An, G.F. Zeng, J.K. Feng, Y.T. Qian, Room-Temperature Liquid Metal Confined in MXene Paper as a Flexible, Freestanding, and Binder-Free Anode for Next-Generation Lithium-Ion Batteries, Small 15 (2019) 1903214.
[49] C.W. Ong, H. Huang, B. Zheng, R.W.M. Kwok, Y.Y. Hui, W.M. Lau, X-ray photoemission spectroscopy of nonmetallic materials: Electronic structures of boron and B_xO_y, J. Appl. Phys. 95 (2004) 3527–3534.
[50] P.G. de Gennes, Wetting: statics and dynamics, Rev. Mod. Phys 57 (1985) 827–863.
[51] W.L. Ma, H.X. Wang, A. Neville, Y. Hua, Understanding the Corrosion Behaviour of Steel Under Alternate Oil/Water Wetting with Different Oil Viscosities, J. Electrochem. Soc. 171 (2024) 031505.
[52] Z. Xia, W. Hu, Y. Xiang, C. Lü, Boron-doped carbon dots modified zirconium porphyrin MOFs enable efficient and highly selective photosynthesis of hydrogen peroxide in water and seawater, Appl. Catal. B-Environ. Energy 358 (2024) 124394.
[53] C.C. Fan, W.J. Meng, D.S. Li, L. Jiang, Stratified adsorption strategy facilitates highly stable dendrite free zinc metal anode, Energy Storage Mater. 56 (2023) 468–477.
[54] S.Z. Qiao, J.Q. Zhou, D.Y. Zhao, G.B. Sun, W.M. Zhang, Q.C. Zhu, constructing amphipathic molecular layer to assists de-solvation process for dendrite-free Zn anode, J. Colloid Interface Sci. 653 (2024) 1085–1093.
[55] H. Xia, G. Xu, X. Cao, C.Y. Miao, H.N. Zhang, P.Y. Chen, Y. Zhou, W. Zhang, Z. M. Sun, Single-Ion-Conducting Hydrogel Electrolytes Based on Slide-Ring Pseudo-Polyrotaxane for Ultralong-Cycling Flexible Zinc-Ion Batteries, Adv. Mater. 35 (2023) 2301996.
[56] D.D. Wang, H.X. Liu, D. Lv, C. Wang, J. Yang, Y.T. Qian, Rational Screening of Artificial Solid Electrolyte Interphases on Zn for Ultrahigh-Rate and Long-Life Aqueous Batteries, Advanced Materials 35 (2023) 2207908.